Title

Dynamic Testing of Alfred Zampa Memorial Bridge

Journal

Journal of Structural Engineering, ASCE, 134(6)

ISSN

0733-9445

Authors

Conte, Joel P

He, Xianfei

Moaveni, Babak

et al.

Publication Date

2008-06-01

DOI

10.1061/(ASCE)0733-9445(2008)134:6(1006)

Peer reviewed

Dynamic Testing of Alfred Zampa Memorial Bridge

Joel P. Conte[1], Member, ASCE, Xianfei He[2], Babak Moaveni[3], Sami F. Masri[4], John P. Caffrey[5], Mazen Wahbeh[6], Farzad Tasbihgoo[7], Daniel H. Whang[8], and Ahmed Elgamal[9], Member, ASCE

Abstract

This paper describes a set of dynamic field tests performed on the Alfred Zampa Memorial Bridge (AZMB), also known as the New Carquinez Bridge, which is located 32km northeast of San Francisco on interstate Highway I-80. The AZMB, opened to traffic in November 2003, is the first suspension bridge in the United States with an orthotropic steel deck, reinforced concrete towers and large-diameter drilled shaft foundations. The dynamic field tests described herein were conducted just before the bridge opening to traffic. They included ambient vibration tests, mainly wind-induced, and forced vibration tests based on controlled traffic loads and vehicle-induced impact loads. Four different controlled traffic load patterns and seven different vehicle-induced impact load configurations were used in the forced vibration tests. The dynamic response of the bridge was measured through an array of 34 uni-axial and 10 tri-axial force-balanced accelerometers deployed along the whole length of the bridge. These dynamic field tests provided a unique opportunity to determine the dynamic (modal) properties of the bridge in its as-built

[1] Corresponding author, Professor, Department of Structural Engineering, University of California at San Diego, 9500 Gilman Drive, La Jolla, California 92093-0085, USA; E-mail: jpconte@ucsd.edu ; Tel: 858-822-4545; Fax: 858-822-2260

[2] Graduate Student, Department of Structural Engineering, University of California at San Diego, 9500 Gilman Drive, La Jolla, California 92093-0085, USA; E-mail: x1he@ucsd.edu

[3] Graduate Student, Department of Structural Engineering, University of California at San Diego, 9500 Gilman Drive, La Jolla, California 92093-0085, USA; E-mail: bmoaveni@ucsd.edu

[4] Professor, Department of Civil and Environmental Engineering, University of Southern California, 3620 South Vermont, Los Angeles, California 90089-2531, USA; E-mail: masri@usc.edu

[5] Associate Professor, Department of Mechanical Engineering, California State Polytechnic University, 3801 West Temple Avenue, Pomona, California 91768, USA; E-mail: jpcaffrey@csupomona.edu

[6] Associate Professor, Department of Civil Engineering, California State Polytechnic University, 3801 West Temple Avenue, Pomona, California 91768, USA; E-mail: amwahbeh@csupomona.edu

[7] Assistant Professor, Department of Civil Engineering, California State Polytechnic University, 3801 West Temple Avenue, Pomona, California 91768, USA; E-mail: ftasbihgoo@csupomona.edu

[8] Exponent Failure Analysis Associates, Engineer, 320 Goddard, Suite 200, Irvine, California 92618; E-mail: dwhang@exponent.com

[9] Professor, Department of Structural Engineering, University of California at San Diego, 9500 Gilman Drive, La Jolla, California 92093-0085, USA; E-mail: elgamal@ucsd.edu

(baseline) condition with no previous traffic loads or seismic excitation. Such properties could be used to validate and/or update the finite element models used in the design phase of this bridge. They could also be used as baseline for future health monitoring studies of this bridge. At the end of the paper, the ambient vibration test data were used to identify the bridge modal parameters (natural frequencies, damping ratios and mode shapes) using the data-driven stochastic subspace identification method.

CE Database subject headings: Alfred Zampa Memorial Bridge; suspension bridge; dynamic field tests; modal parameters; system identification; stochastic subspace identification.

Introduction

Dynamic field testing is the most reliable method to determine the true dynamic properties (e.g., natural frequencies, damping ratios and mode shapes) of a structure, which can then serve as a basis for validating and/or updating analytical models of that structure so that these models represent the actual structural properties and boundary conditions. Furthermore, the dynamic characteristics extracted from dynamic response measurements are also essential for vibration-based structural health monitoring (Doebling et al. 1996; Sohn et al. 2003)..

Dynamic tests of bridges are usually subdivided into two types: forced and ambient vibration tests. Forced vibration tests are directly related to the application of classical experimental modal analysis (Ewins 2003), in which the bridge is usually excited by artificial means such as eccentric or linear inertial shakers (Halling et al. 2001; Brownjohn et al. 2003) or drop weights (Abdel Wahab and De Roeck 1998). A sudden impact on the bridge induces a condition of free vibration. In previous experimental studies, some creative methods have been employed to generate impact loads in dynamic testing of bridges. For example, in a study by Delaunay et al. (1999), the horizontal impulsive force was generated by the sudden release of a tension cable that connected the bridge to a tug-boat. In another study by Huang et al. (1999), impact forces in the longitudinal and transverse directions were generated by the sudden braking of a truck at a specified location on the bridge, whereas vertical impact forces were generated by simply letting the rear wheels of the truck drop from the top of a concrete block. Earthquake excitation (when

measured) provides a natural source of forced vibration for bridge and other civil structures (Smyth et al. 2003).

In general, forced vibration tests provide more accurate modal identification results than ambient vibration tests, since (a) well-defined input excitations are used in the modal identification procedure, and (b) the excitations can be optimized to enhance the response of the vibration modes of interest. However, in the case of large and flexible bridges (such as suspension and cable-stayed bridges) with natural frequencies of the predominant modes in the range 0-1Hz, it is challenging and costly to provide controlled excitation for significant level of response.

In contrast, ambient vibration tests take advantage of "free" or natural excitation sources such as traffic, wind, micro-tremors and combinations thereof. Moreover, since ambient vibration tests do not interrupt service of the test structure (e.g., shutting down traffic during bridge testing), they can be used readily for long term continuous structural health monitoring applications. Ambient vibration tests have been successfully applied to a variety of bridge structures such as the Vincent Thomas suspension bridge (Abdel-Ghaffar and Housner, 1978), Golden Gate suspension bridge (Abdel-Ghaffar and Scanlan 1985), Roebling suspension bridge (Ren et al. 2004a), Safti Link curved cable-stayed bridge (Brownjohn et al. 1999), Vasco da Gama cable-stayed bridge (Cunha et al. 2001), twin curved cable-stayed bridges on the north and south sides of Malpensa airport in Milan (Gentile and Martinez y Cabrera 2004), Brent-Spence truss bridge (Harik et al. 1997) and Tennesse River steel arch bridge (Ren et al. 2004b). In these studies, system identification based on ambient vibration test data provided accurate estimates of natural frequencies and mode shapes despite the relatively low amplitude of the measured vibrations. Even though modal damping ratios/factors can be satisfactorily identified using ambient vibration data, they typically require the use of advanced system identification methods due to the low amplitude and relatively low signal-to-noise ratio of such data. Therefore, results on identification of modal damping ratios using ambient vibration data are scarce.

This paper describes in detail a set of dynamic tests performed on the Alfred Zampa Memorial Bridge (AZMB). They include ambient vibration tests (mainly wind-induced) and forced vibration tests based on

controlled traffic loads and vehicle-induced impact loads. The vibration response of the bridge was measured using an array of 34 uni-axial and 10 tri-axial force-balanced accelerometers from the mobile field laboratory of the George E. Brown, Jr. Network for Earthquake Engineering Simulation (NEES) field testing site at the University of California at Los Angeles (NEES@UCLA). These accelerometers were installed at 25 selected stations along both sides of the bridge deck. Instead of roving accelerometers around to the different measurement stations with fixed accelerometers at one or more reference stations (as commonly done for dynamic testing of bridges), a total of 64 channels of acceleration response data were recorded simultaneously in the tests described here, including 25 vertical, 25 transversal, and 14 longitudinal motion components. These dynamic field tests are the first ones conducted on the AZMB, and they were performed just before the bridge opening to traffic. Therefore, these tests provided a unique opportunity to determine the dynamic properties of the bridge in its as-built (baseline) condition with no previous traffic loads or seismic excitation.

The scope of this paper is two-fold: (1) describe in detail the dynamic field tests performed on the AZMB including the sensor network/array, data acquisition system and dynamic test procedure; (2) present some modal identification results obtained using a state-of-the-art time domain system identification method applied to the ambient vibration data. Sections 2 and 3 describe the AZMB, and sensor layout and data acquisition system used in the dynamic tests, respectively; Section 4 presents the testing procedure; Section 5 briefly describes the system identification method used and presents the modal identification results obtained; and Section 6 provides some concluding remarks.

Bridge Description

The Carquinez Strait, located about 32km northeast of San Francisco, carries the Sacramento River into San Francisco Bay. Before the construction of the AZMB, the strait was spanned by two steel truss bridges, built in 1927 and 1958, respectively, which provide a vital link on the interstate Highway I-80 corridor. The AZMB is the third bridge crossing the Carquinez Strait (see Fig. 1) and will replace the original bridge that was built in 1927. With a main span of 728m and side spans of 147m and 181m, the AZMB is the first major suspension bridge built in the United States (US) since the 1960s. The design

and construction of the AZMB incorporates several innovative structural features that have never been used previously for a suspension bridge in the US, namely (1) orthotropic (aerodynamic) steel deck; (2) reinforced concrete towers; and (3) large-diameter drilled shaft foundations. The AZMB is also the first suspension bridge in the world with concrete towers in a high seismic zone.

The closed steel box girder with orthotropic deck provides a light weight, durable, and low-maintenance alternative to the stiffening trusses that have been used on previous suspension bridges in the US. It is continuous through the towers, with expansion joints located only at the far ends of the side spans. Its slender 3m depth allows adequate navigation clearance without excess structure height. Its shape was developed in a wind tunnel to provide aerodynamic stability and low drag. Its rigidity against bending and torsion contributes to superior bridge performance under wind, seismic, and traffic loads. Its closed form, with smooth outside surfaces and stiffening elements located inside, reduces maintenance costs.

The reinforced concrete towers rising about 125m above the mean water level are the prominent architectural feature of the bridge. The ductile frames formed by the tower shafts and their connecting struts provide a “rectangle of air” above drivers. This is the first application of concrete towers on a suspension bridge in the US, and to any suspension bridge in the world in a high seismic risk zone. The cellular shafts incorporate spirally reinforced corner pilasters to improve ductility and provide architectural relief. The towers were designed to a seismic standard requiring essentially elastic behavior in the maximum credible earthquake (as defined in Caltrans’ seismic design procedures), with some limited inelastic behavior allowed in their lower sections. Drilled shaft foundations support pile caps on which the towers were built. Steel casings were driven through overlying sediments into the top of the rock. Then an uncased rock socket was drilled below the casing. The rock socket and casing were then reinforced and concreted. Each tower is supported by twelve such shafts, with a maximum length of about 90m. These foundations are economical to build, have less impact on water flow than large sunken caissons, and were designed to the same seismic standard as the towers.

The south transition pier supports the end of the steel deck girder, houses tie-downs that divert the geometry of the cables to the south anchorage, and supports the end of the south viaduct. It is structurally and architecturally similar to the main towers, with cellular reinforced concrete shafts and pile foundations. The south cable anchorage transfers the thrust of the cables to the ground via massive concrete anchor blocks and a combination of batter piles and vertical piles. The splay chambers rise 18m above ground, while the anchor blocks extend about 10m beneath the ground surface. The north cable anchorage transfers the thrust of the cables to the ground by direct bearing on the underlying rock, and also serves as a bridge abutment. The concrete anchor blocks and splay chambers are benched into the rock beneath the roadway and only the relatively small saddle housings are exposed. More details about this bridge such as the special engineering studies and structural quantities can be found elsewhere (Ketchum 2006; Caltrans 2006).

Description of Instrumentation and Data Acquisition System

NEES@UCLA Data Acquisition Equipment

Equipment from NEES@UCLA was used to perform the dynamic tests on the AZMB. The NEES@UCLA field mobile laboratory deployed for this study consisted of:

1. EpiSensor accelerometers from Kinemetrics Inc. including both EpiSensor ES-U (uni-axial) and EpiSensor ES-T (tri-axial). The EpiSensor force-balanced accelerometers have a wide frequency bandwidth from DC (i.e., 0Hz) to 200Hz, a large amplitude range (user selectable at $\pm 0.25g, \pm 0.5g, \pm 1g, \pm 2g, \pm 4g$) set at $\pm 2g$ for these experiments, and a broad dynamic range (140dB+ for ES-U and 155dB+ for ES-T). The significant bandwidth (from DC to 200Hz) allows for the study of motions at higher frequencies while maintaining the very important low frequency and DC response needed in field calibration, in post-processing of the data (e.g., double integration of acceleration records) and in studying the low frequency predominant modes of the AZMB.
2. Quanterra Q330 data loggers from Kinemetrics, Inc., to provide signal conditioning (e.g., anti-aliasing filter), analog to digital (A/D) conversion, GPS (i.e., global positioning system) time stamping for synchronization across multiple nodes, local memory buffer and IP-network (i.e., Internet Protocol

network) communication capabilities via hardwire or wireless. The nominal performance specifications for the Q330 data loggers include 24-bit A/D resolution, 135dB dynamic range, and a time stamp (time synchronization) accuracy of < 0.1ms.

3. Antelope data acquisition software (Boulder Real Time Technologies 2006) for real-time monitoring and recording of data. A data concentrator which consists of a field-ruggedized UNIX workstation running Antelope, networking switches and wireless communication radios, was used to centrally record the data from each of the Q330 data logger nodes.
4. Mobile command center containing computing facilities, satellite uplink (not used in these tests) and equipment storage.

Collectively, the NEES@UCLA field data acquisition system represents the state-of-the-art in seismic monitoring equipment. The accelerometers transmit analog signals to the Q330 data loggers in which they are digitized, time-stamped and stored in a local memory buffer as data packets. From there, the data packets are sent to the data concentration point using Transmission Control Protocol/Internet Protocol (TCP/IP) with either Ethernet cables or IEEE 802.11b, a standard for local area networks from the Institute of Electrical and Electronic Engineers (IEEE), long-range wireless radios. Ethernet cables were used for this experiment due to external radio frequency interference which limited drastically the transmission distance of the wireless equipment. The data concentration point contains a Sun Microsystems Netra 120 server (a high density, thin, ruggedized server designed to withstand extreme levels of temperatures, humidity, radiation and vibrations) running Antelope data acquisition software to centrally record data packets received from each of the various Quanterra Q330 nodes. Finally, the Antelope server in the data concentration point transmits, using an orb2orb transfer protocol, all of the received data packets to a laptop computer inside the mobile command center also running Antelope software. The laptop computer was used to observe the experiment in real-time using the Antelope real-time monitoring (Antelope RTM) system. Fig. 2 illustrates the network of the NEES@UCLA field mobile laboratory.

Accelerometer Layout

The mobile command center was located near midpoint of the bridge main span and the accelerometers were installed at selected locations (stations) along both sides of the bridge deck covering the whole length of the bridge. Along the west side of the bridge deck, 14 stations were instrumented with either a single EpiSensor ES-T (tri-axial) or three EpiSensors ES-U (uni-axial) at each station to measure the vertical, transversal and longitudinal motion components. The east side of the bridge deck was instrumented with 22 EpiSensors ES-U at 11 stations (i.e., two uni-axial accelerometers per station) measuring the vertical and transversal motion components. Fig. 3 shows the sensor locations along the bridge deck. At each station, the accelerometers were mounted on a square aluminium plate of size $203 \times 203 \times 6$ (mm). These plates were attached to the bridge deck using semi-permanent adhesive sheets providing the required stiffness between the plates and the deck. Each Q330 has two 3-channel ports (A and B) to connect sensors. A hub was used to connect up to three EpiSensors ES-U to each port. Due to a limited number of hubs available at the time of the experiments and the narrow time window available to perform the experiments, acceleration responses at stations 6SW (i.e., station 6 at southwest side of the bridge deck), 6SE, 7SE, 6NE and 7NE (see Fig. 3) could not be recorded.

Dynamic Tests Performed on the Bridge

Three types of excitation sources were used for the dynamic field tests performed on the AZMB: controlled traffic loads, vehicle-induced impact loads and wind. The controlled traffic loads consisted of two heavy trucks weighing 405kN (Truck A) and 409kN (Truck B), respectively, traversing the bridge at specified velocities and the impact loads were generated using one or both of these trucks driving over triangular shaped steel ramps (60cm long and 10cm high) designed and constructed specifically for these tests. The vehicle-induced impact excitation was intended to induce a free vibration response significantly higher than the ambient vibration response (mainly wind-induced) and the response to the controlled traffic loads. Four controlled traffic load patterns were defined in the controlled traffic loads and vehicle-induced impact tests, namely: (I) two trucks crossing over the bridge in parallel (Fig. 4a); (II) two trucks crossing over the bridge in opposite direction (Fig. 4b); (III) one truck crossing over the bridge; and (IV)

two trucks crossing over the bridge following each other in the same traffic lane. It should be mentioned that the trucks could only use the two middle traffic lanes (see Fig. 4) during the tests.

Controlled Traffic Load Tests

The first three controlled traffic load patterns were used as the excitation sources in this set of tests. For each traffic load pattern, two specified truck velocities were used, namely 24km/h and 48km/h. Due to the end-of-construction field condition at the time of the tests, the trucks could be driven at the specified velocities only along the main span of the bridge (between the two towers). During the tests, the trucks were commanded through radio communication from the mobile command center, located near midpoint of the main span, where the data were monitored in real-time and recorded. Table 1 provides a detailed description of the controlled traffic load tests. As an illustration, Fig. 5 shows the vertical acceleration response at the midpoint, south quarter point and near the south end of main span on the west side of the bridge deck (i.e., stations 0W, 3SW, and 5SW) measured in Test No. 5, during which one truck crossed over the bridge from north to south on the west traffic lane. Notice that a peak vertical bridge deck acceleration of about 0.01g is observed during this test. The Fourier amplitude spectrum of the vertical response measured at station 3SW is shown in Fig. 6. For a long-span suspension bridge such as the AZMB, the lower modes natural frequencies are below 1Hz. It is observed from Fig. 6 that during the controlled traffic load tests, the vibration modes with natural frequencies above 1Hz (higher vibration modes) are more significantly excited than those with natural frequencies below 1Hz (lower vibration modes).

Vehicle-induced Impact Tests

Two pairs of triangular shaped steel ramps were used in the vehicle-induced impact tests. As an illustration, Fig. 7 shows two pairs of steel ramps set up along the centerline of the bridge main span. In this set of tests, all of the four controlled traffic load patterns defined above were used in combination with seven different ramp configurations: (a) two pairs of ramps located at midpoint of main span; (b) a single pair of ramps located at midpoint of main span on the west traffic lane; (c) a pair of ramps located at the north quarter point of main span on the west traffic lane and the second pair located at midpoint of

main span on the east traffic lane; (d) one pair of ramps located at the north quarter point of main span on the west traffic lane and the second pair located at the south quarter point of main span on the east traffic lane; (e) a single pair of ramps located at the north quarter point of main span on the west traffic lane; (f) a pair of ramps located at both the north and south quarter points of main span on the east traffic lane; and (g) a pair of ramps located at both the north quarter point and midpoint of main span on the west traffic lane. The trucks approached the ramps at the specified velocity of 32km/h, but traversed the ramps at the reduced velocity of 8km/h. For safety reason, one of the trucks crossed over the ramps at very low velocity (less than 1km/h). Details of these tests are provided in Table 2. As an illustration, Fig. 8 shows the vertical bridge deck acceleration response at the midpoint, south quarter point and near the south end of main span on the west side of bridge deck (i.e., stations 0W, 3SW, and 5SW) measured in Test No. 10, during which both trucks crossed over the bridge in opposite direction with two pairs of ramps located at midpoint of main span. Notice that a peak vertical bridge deck acceleration of about 0.08g is observed during this test, which is significantly larger than that observed in Test No. 5 (peak acceleration of 0.01g). Fig. 9 shows the Fourier amplitude spectra of the vertical acceleration response measured at station 3SW in Test No. 10 and Test No. 12, during which both trucks crossed over the bridge in opposite direction with two pairs of ramps located at the north quarter point of main span on the west traffic lane and the south quarter point of main span on the east traffic lane, respectively. It is clearly seen that the relative contributions of the bridge vibration modes to the measured response depends on the locations of the steel ramps (i.e., the locations of the impact loads). However, in both cases (Test No. 10 and Test No. 12) the higher vibration modes were excited much more significantly than the lower vibration modes.

At the end of the sequence of vehicle-induced impact tests, the response of the bridge was measured due to longitudinal forces applied on the bridge deck. These forces were generated through braking of the trucks while they were crossing over the bridge in parallel from south to north (Test No. 16). In this test, for safety consideration, the drivers applied normal and not hard breaks on the trucks to stop at midpoint of main span.

Ambient Vibration Tests

Ambient vibration tests were conducted after completion of all the tests based on the two trucks in traffic condition, just after midnight local time, while there were no construction activities on the bridge and thus bridge vibrations were induced mainly by wind. Two cases of ambient vibration tests were performed: the bridge response was measured (1) when both trucks were stationed at midpoint of main span (Test No. 17), and (2) after both trucks left the bridge (Test No. 18). As an illustration, Fig. 10 shows the vertical acceleration response at the midpoint, south quarter point and near the south end of main span on the west side of the bridge deck (i.e., stations 0W, 3SW, and 5SW) measured in Test No. 18. Notice that a peak vertical bridge deck acceleration of about 0.003g is observed during this test, which is much smaller than that observed in Test No. 5 (controlled traffic load tests), see Fig. 5. The Fourier amplitude spectrum of the vertical acceleration response measured at station 3SW is shown in Fig. 11. During Test No. 18, the vibration modes below 1Hz were excited as much as those above 1Hz. Despite the fact that the amplitude of the measured ambient vibration response is much lower than that of the forced vibration response measured, the ambient vibration data was found to be very clean (i.e., high signal-to-noise ratio, see Fig. 11), especially for identifying the lower vibration modes.

Modal Identification Using Data-driven Stochastic Subspace Identification

Since the response only of the bridge was measured (i.e., un-measured input) during the dynamic tests, the system identification procedure used herein is based on output-only measurements. Thus, the data-driven Stochastic Subspace Identification (SSI-DATA) method is applied to extract the properties of the bridge lower vibration modes from the 20 minutes long ambient vibration data measured from the main span during Test No. 18. SSI-DATA is one of the most advanced state-of-the-art output-only system identification method, which has already been successfully applied for modal parameter identification of long span bridges based on ambient vibration data (Ren et al. 2004b). The SSI-DATA algorithm extracts a system model in state-space using output-only measurement data directly (Van Overschee and De Moor 1996; Peeters and De Roeck 2001). Compared to two-stage time-domain system identification methods such as covariance-driven stochastic subspace identification (SSI-COV) (Van Overschee and De Moor 1996) and the natural excitation technique (NExT) (James et al. 1993) combined with the eigensystem

realization algorithm (ERA) (Juang and Pappa 1985), SSI-DATA does not require any pre-processing of the data to calculate auto/cross-correlation functions or auto/cross-spectra of output data. In addition, robust numerical techniques such as QR factorization, singular value decomposition (SVD) and least squares are involved in this method.

In each test, the measured bridge acceleration response was sampled at the rate of 200Hz resulting in a Nyquist frequency of 100Hz, which is much higher than the bridge natural frequencies of interest (< 1Hz in this study). In applying SSI-DATA, the measured data were first low-pass filtered below 1Hz using a Butterworth infinite impulse response (IIR) filter of order 7 and then down-sampled to 10Hz in order to improve the computational efficiency of SSI-DATA. After re-sampling, the Nyquist frequency (5Hz) is still much higher than the natural frequencies of interest (< 1Hz). An output Hankel matrix is formed including 100 block rows with 21 rows in each block (21 vertical channels) using the down-sampled low-pass filtered vibration data. The identified natural frequencies and damping ratios of the first 12 vibration modes in the frequency range below 1Hz are reported in Table 3. The identified modal damping ratios are very low, but are consistent with the results of previous system identification studies of long span suspension bridges based on ambient vibration data (Abdel-Ghaffar and Housner 1978). In other system identification studies of a long span suspension bridge (Niazy 1991), modal damping ratios estimated using ambient vibration data were found significantly smaller than their counterparts estimated using seismic data.

The vibration mode shapes identified using state-of-the-art time domain system identification methods such as SSI-DATA used here are usually complex valued. Fig. 12 presents the identified mode shapes for the first 12 vibration modes of the AZMB (main span only) as vectors in the complex plane (also called polar plots). These polar plots have the advantage to show directly the extent of the non-proportional damping characteristics of a vibration mode. If all complex valued components of a mode shape vector are collinear (in phase or 180 degrees out of phase), the vibration mode is classically (or proportionally) damped. On the other hand, the more these mode shape components are scattered in the complex plane, the more the vibration mode is non-classically (or non-proportionally) damped. Measurement noise (i.e.,

poor signal-to-noise ratio due to low modal participation), estimation errors, and modeling errors could also cause a "true" classically damped mode to be identified as non-classically damped. Fig. 12 shows that all the identified modes are either perfectly or nearly classically damped. A three-dimensional (3D) representation of the normalized mode shapes of these 12 modes is given in Fig. 13. Normalization was performed through dividing all mode shape components by the component of largest magnitude and then projecting all components onto the real axis. The identified space-discrete mode shapes were interpolated between the sensor locations using cubic splines along both sides of the bridge deck and straight lines along the deck transverse direction. Since the accelerometers at stations 6SW, 6SE, 7SE, 6NE and 7NE could not be recorded, the vibration mode shapes were plotted over the main span only and are based on the assumption that the motion of the bridge deck at the towers is restrained in the vertical direction. In addition, the vertical acceleration response at station 5SE was not recorded properly in the tests, and the mode shape components at stations 5NE and 5SW were used to represent the component at station 5SE. It can be seen that the 5^{th} and 8^{th} identified mode shapes (observed only over the main span in this study) are neither symmetric nor anti-symmetric with respect to the midpoint of the deck. Additional measurement stations on the towers and approach spans (which have different lengths) would be needed to identify the corresponding global bridge mode shapes.

Summary and Conclusions

This paper presents a set of dynamic field tests performed on the Alfred Zampa Memorial Bridge located 32km northeast of San Francisco on interstate Highway I-80, just before its opening to traffic in November 2003. These tests provided a unique opportunity to obtain the dynamic properties of the bridge in its as-built condition with no previous traffic loads or seismic excitation.

The dynamic field tests included ambient vibration tests (mainly wind-induced) and forced vibration tests based on controlled traffic loads and vehicle-induced impact loads. The controlled traffic loads consisted of two heavy trucks traversing the bridge at specified velocities and the impact loads were generated using one or both of these trucks driving over small steel ramps designed and constructed specifically for these tests. During the vibration tests, the dynamic response of the bridge was measured

using an array of 34 uni-axial and 10 tri-axial force-balanced accelerometers. These accelerometers were installed at 25 selected stations along both sides of the bridge deck, covering the whole length of the bridge main span. Instead of roving accelerometers around to the different measurement stations with fixed accelerometers at one or more reference stations (as typically done in the past), a total of 64 channels of acceleration response data were recorded simultaneously in the dynamic field tests described here, including 25 vertical, 25 transversal, and 14 longitudinal motion components.

During the forced vibration tests, the vibration modes with natural frequencies above 1Hz were more significantly excited than those with natural frequencies below 1Hz, which renders the lower vibration modes of the bridge (< 1 Hz) more difficult to identify. During the ambient vibration tests, the bridge was excited mainly by the wind which provided a broadband excitation. The lower vibration modes (< 1Hz) and some higher modes (> 1 Hz) were excited almost at the same level. Therefore, the ambient vibration data was found to be more informative for identification of the lower vibration modes. In addition, even though the amplitude of the measured ambient vibration response is very low (0.003g peak acceleration), the recorded data was found to be very clean (i.e., data has high signal-to-noise ratio).

Finally, using the vibration data acquired during the ambient vibration test, the first 12 vibration modes (natural frequencies, damping ratios, and mode shapes) were identified using the data-driven stochastic subspace identification method. It is found that (1) all the identified modes presented in this study are either perfectly or nearly classically damped; and (2) the identified modal damping ratios are found to be very low (in the range 0.1-0.3% for most lower modes). However, these low identified damping ratios are consistent with the results of previous system identification studies of long span suspension bridges based on ambient vibration data. More comprehensive system identification studies using different system identification methods and different types of test data as well as comparisons between identified modal properties with their counterparts computed from a detailed 3D finite element model of the bridge (used in the design of the AZMB) are being performed by the authors based on the test data presented in this paper.

Acknowledgements

Support of this research by the National Science Foundation under ITR Grant No. 0205720 is gratefully acknowledged. The joint UCSD-USC-UCLA research team who conducted the dynamic field tests reported and studied in this paper were assisted by several individuals and organizations: Brian Boal (Caltrans), Louis Bates (Caltrans Consultant Engineer), Joe Reyes (Caltrans), and Frank Daams (FCI/Cleveland Bridge). Their help is very much appreciated. The authors are also thankful to Mark Ketchum (OPAC Consulting Engineers) for very useful and interesting discussions about the conception and design of the Alfred Zampa Memorial Bridge. Any opinions, findings, and conclusions or recommendations expressed in this material are those of the authors and do not necessarily reflect those of the sponsor.

References

Abdel-Ghaffar, A. M., and Housner, G. W. (1978). "Ambient vibration tests of suspension bridge." *Journal of the Engineering Mechanics Division*, ASCE, 104(5), 983-999.

Abdel-Ghaffar, A. M., and Scanlan, R. H. (1985). "Ambient vibration studies of Golden Gate Bridge: I. suspended structure." *Journal of Engineering Mechanics*, ASCE, 111(4), 463-482.

Abdel Wahab, M. M., and De Roeck, G. (1998). "Dynamic testing of prestressed concrete bridges and numerical verification." *Journal of Bridge Engineering*, ASCE, 3(4), 159-169.

Boulder Real Time Technologies (2006). *Antelope Release 4.8* <http://www.brtt.com>. Boulder Real Time Technologies, Inc, Boulder, Colorado.

Brownjohn, J. M. W., Lee, J., and Cheong B. (1999). "Dynamic performance of a curved cable-stayed bridge." *Engineering Structures*, 21(11), 1015-1027.

Brownjohn, J. M. W., Moyo, P., Omenzetter, P., and Lu, Y. (2003). "Assessment of highway bridge upgrading by dynamic testing and finite- element model updating." *Journal of Bridge Engineering*, ASCE, 8(3), 162-172.

California Department of Transportation (Caltrans), (2006). "The New Carquinez Bridge." <http://www.dot.ca.gov/dist4/carquinez.htm> (August 15, 2006).

Cunha, A., Caetano, E., and Delgado, R. (2001). "Dynamic tests on large cable-stayed bridge." *Journal of Bridge Engineering*, ASCE, 6(1), 54-62.

Delaunay D., Grillaud, G., Bietry, J., and Sacre, C. (1999). "Wind response of long span bridges: in-situ measurements and modal analysis." *Proceedings of the 17th International Modal Analysis Conference*, Kissimmee, Florida, 719-725.

Doebling, S. W., Farrar, C. R., Prime, M. B., and Shevitz, D. W. (1996). "Damage identification and health monitoring of structural mechanical systems from changes in their vibration characteristics: A literature review." *Report No. LA-13070-MS*, Los Alamos National Laboratory, Los Alamos, New Mexico.

Ewins, D. J. (2003). *Modal Testing: Theory, Practice and Application*, Research Studies Press, Baldock, UK.

Gentile, C., and Martinez y Cabrera, F. (2004). "Dynamic performance of twin curved cable-stayed bridges." *Earthquake Engineering and Structural Dynamics*, 33(1), 15-34.

Halling, M. W., Muhammad, I., and Womack, K. C. (2001). "Dynamic testing for condition assessment of bridge bents." *Journal of Structural Engineering*, ASCE, 127(2), 161-167.

Harik, I. E., Allen, D. L., Street, R. L., Guo, M., Graves, R. C., Harison, J., and Gawry, M. J. (1997). "Free and ambient vibration of Brent-Spence Bridge." *Journal of Structural Engineering*, ASCE, 123(9), 1262-1268.

Huang, C. S., Yang, Y. B., Lu, L. Y., and Chen C. H. (1999). "Dynamic testing and system identification of a multi-span highway bridge." *Earthquake Engineering and Structural Dynamics*, 28(8), 857-878.

James, G. H., Carne, T. G., and Lauffer, J. P. (1993). "The natural excitation technique for modal parameters extraction from operating wind turbines." *Report No. SAND92-1666, UC-261*, Sandia National Laboratories, Sandia, New Mexico.

Juang, J. N., and Pappa, R. S. (1985). "An eigensystem realization algorithm for modal parameter identification and model reduction." *Journal of Guidance, Control and Dynamics*, 8(5), 620-627.

Ketchum, M. (2006). "Carquinez Strait Bridge page." <http://www.ketchum.org/carquinez.html> (August 15, 2006).

Niazy, A. M. (1991). "Seismic performance evaluation of suspension bridges." Ph.D. Dissertation, University of Southern California.

Peeters, B., and De Roeck, G. (2001). "Stochastic system identification for operational modal analysis: A review." *Journal of Dynamic Systems, Measurement, and Control*, 123(4), 659-667.

Ren, W. X., Harik, I. E., Blandford, G. E., Lenett, M., and Baseheart, T. M. (2004a). "Roebling suspension bridge. II: Ambient testing and live-load response." *Journal of Bridge Engineerin*g, ASCE, 9(2), 119-126.

Ren, W. X., Zhao, T., and Harik, I. E. (2004b). "Experimental and analytical modal analysis of steel arch bridge." *Journal of Structural Engineering*, ASCE, 130(7), 1022-1031.

Smyth, A.W., Pei, J.-S., and Masri, S.F. (2003). "System identification of the Vincent Thomas suspension bridge using earthquake records," *Earthquake Engineering and Structural Dynamics*, 32(3), 339-367.

Sohn, H., Farrar, C. R., Hemez, F. M., Shunk, D. D., Stinemates, D. W., and Nadler, B. R. (2003). "A review of structural health monitoring literature: 1996-2001." *Report No. LA-13976-MS*, Los Alamos National Laboratory, Los Alamos, New Mexico.

Van Overschee, P., and De Moor, B. (1996). *Subspace Identification for Linear Systems: Theory-Implementation-Applications*, Kluwer Academic Publishers, Norwell, Massachusetts, USA.

Table 1. Controlled traffic load tests

Tests No. Time*	Traffic Pattern	Driving Direction	Velocity (km/h)	Test description
1 04:14:05	Pattern I	From North (N) to South (S)	48	Truck A driving on the west lane and truck B driving on the east lane.
2 04:24:10	Pattern III	From S to N	48	Truck A crossing over the bridge on the west lane.
3 04:30:13	Pattern II	Truck A from N to S; Truck B from S to N	48	Truck A driving on the west lane and truck B driving on the east lane.
4 04:48:41	Pattern II	Truck A from S to N; Truck B from N to S	24	Truck A driving on the east lane and truck B driving on the west lane.
5 04:56:55	Pattern III	From N to S	24	Truck A crossing over the bridge on the west lane.
6 05:04:15	Pattern I	From S to N	24	Truck A driving on the west lane and truck B driving on the east lane.

** The time shown here and in the next table is the Coordinated Universal Time (UTC) (also known as Greenwich Mean Time).*

Table 2. Vehicle-induced impact load tests

Tests No. Time	Traffic Pattern	Driving Direction	Impact Loads	Test description
7 05:55:05	Pattern I	From North (N) to South (S)	Configuration a	Truck A driving on the west lane and truck B driving on the east lane.
8 06:25:13	Pattern I	From S to N	Configuration a	Truck A driving on the west lane and truck B driving on the east lane.
9 06:39:40	Pattern III	From N to S	Configuration b	Truck A crossing over the bridge on the west lane.
10 06:47:32	Pattern II	Truck A from S to N; Truck B from N to S	Configuration a	Truck A driving on the east lane and truck B driving on the west lane.
11 07:12:13	Pattern II	Truck A from N to S; Truck B from S to N	Configuration c	Truck A driving on the west lane and truck B driving on the east lane.
12 07:30:27	Pattern II	Truck A from S to N; Truck B from N to S	Configuration d	Truck A driving on the east lane and truck B driving on the west lane.
13 07:36:10	Pattern III	From N to S	Configuration e	Truck A crossing over the bridge on the west lane.
14 07:54:25	Pattern IV	From S to N	Configuration f	Two trucks following each other to cross over the bridge on the east lane.
15 08:13:20	Pattern IV	From N to S.	Configuration g	Two trucks following each other to cross over the bridge on the west lane.

Table 3. Identified frequencies and damping ratios

	Mode No.	Frequency [Hz]	Damping Ratio [%]
1	1-S-V*	0.193	0.21
2	1-AS-V	0.201	1.36
3	2-S-V	0.258	0.23
4	2-AS-V	0.350	0.20
5		0.414	0.13
6	1-S-T	0.471	0.17
7	3-S-V	0.483	0.21
8		0.561	0.15
9	3-AS-V	0.645	0.11
10	1-AS-T	0.741	0.34
11	4-S-V	0.799	0.23
12	4-AS-V	0.956	0.15

** 1-S-V: 1st Symmetric Vertical mode; S: Symmetric; AS: Anti-Symmetric; V: Vertical; T: Torsional.*

Figure Captions

Fig. 1. Location of the AZMB

Fig. 2. Network diagram of the NEES@UCLA seismic monitoring equipment

Fig. 3. Layout of accelerometers (EpiSensors ES-U and ES-T) along the bridge deck (unit: m)

Fig. 4. Controlled traffic load patterns

Fig. 5. Vertical bridge deck acceleration response measured in Test No. 5

Fig. 6. Fourier amplitude spectrum of vertical acceleration response at station 3SW measured in Test No. 5

Fig. 7. Steel ramps used in the tests

Fig. 8. Vertical bridge deck acceleration response measured in Test No. 10

Fig. 9. Fourier amplitude spectra of vertical acceleration response at station 3SW measured in Tests No. 10 and 12

Fig. 10. Vertical bridge deck acceleration response measured in Test No. 18

Fig. 11. Fourier amplitude spectrum of vertical acceleration response at station 3SW measured in Test No. 18

Fig. 12. Polar plot representation of vibration mode shapes identified using SSI-DATA

Fig. 13. 3D representation of normalized vibration mode shapes identified using SSI-DATA

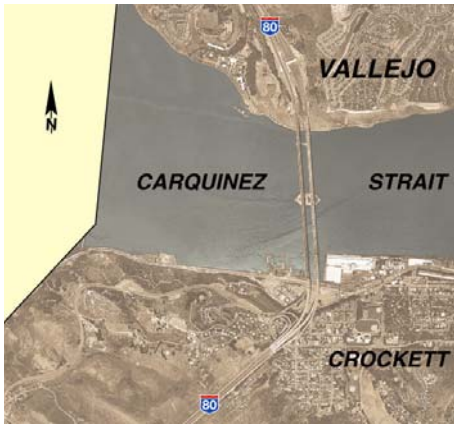

Fig. 1. Location of the AZMB

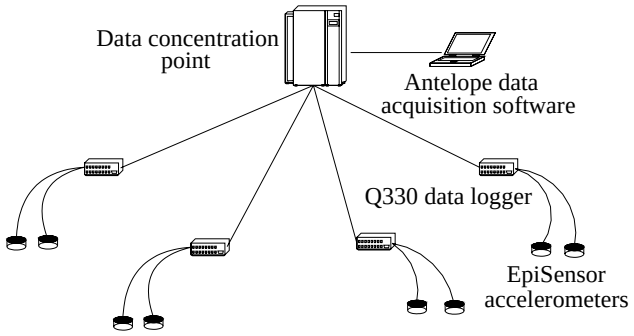

Fig. 2. Network diagram of the NEES@UCLA seismic monitoring equipment

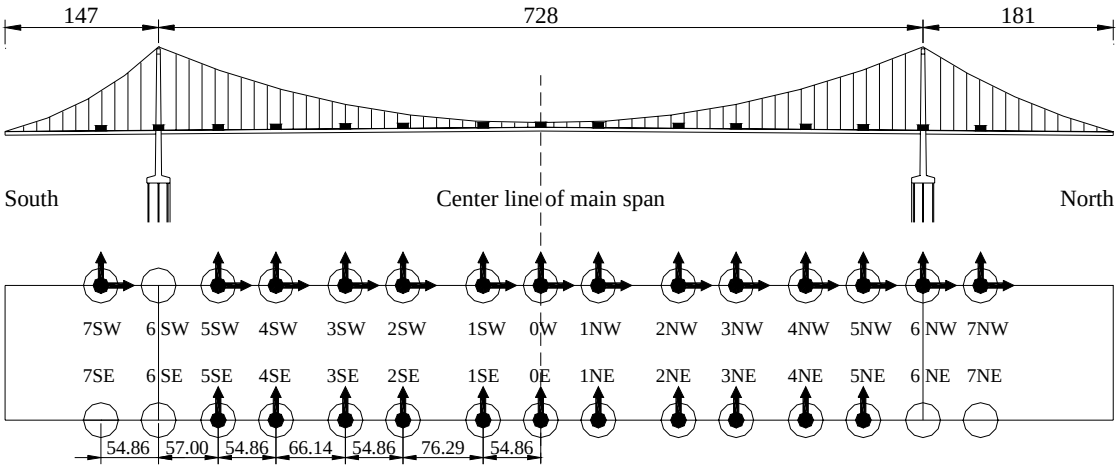

Fig. 3. Layout of accelerometers (EpiSensors ES-U and ES-T) along the bridge deck (unit: m)

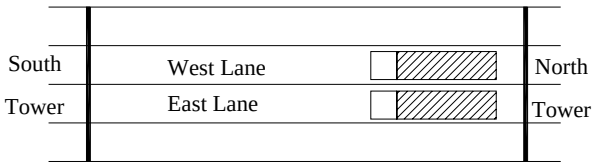

(a) Pattern I

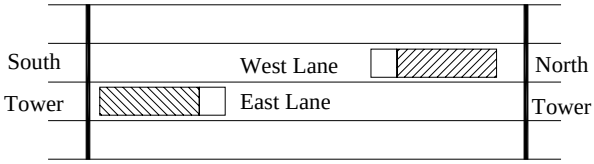

(b) Pattern II

Fig. 4. Controlled traffic load patterns

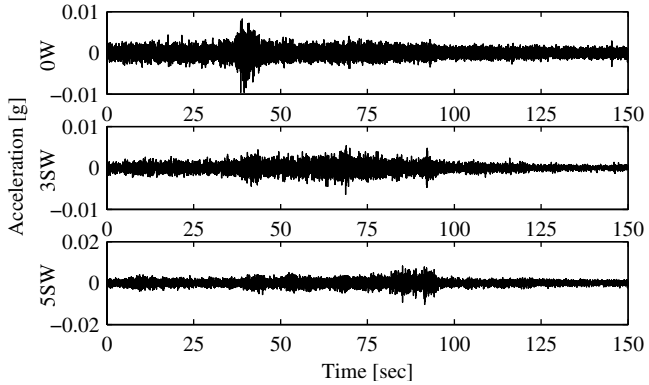

Fig. 5. Vertical bridge deck acceleration response measured in Test No. 5

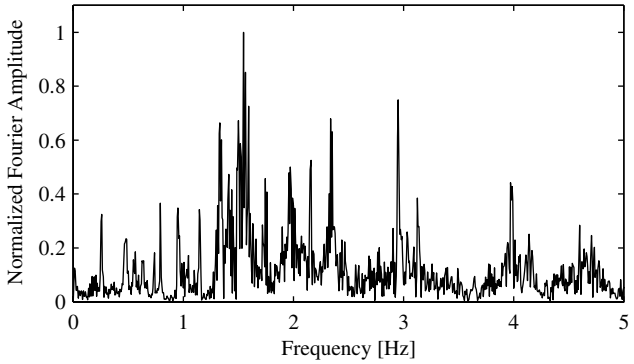

Fig. 6. Fourier amplitude spectrum of vertical acceleration response at station 3SW measured in Test No. 5

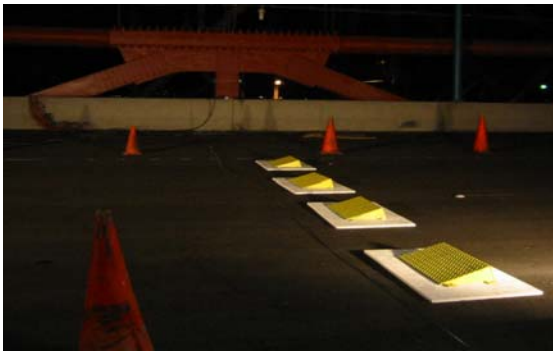

Fig. 7. Steel ramps used in the tests

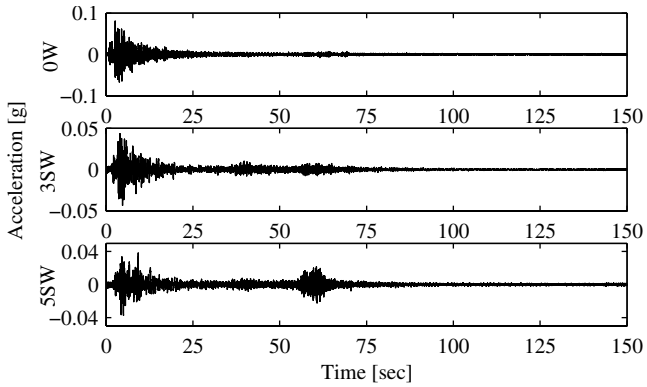

Fig. 8. Vertical bridge deck acceleration response measured in Test No. 10

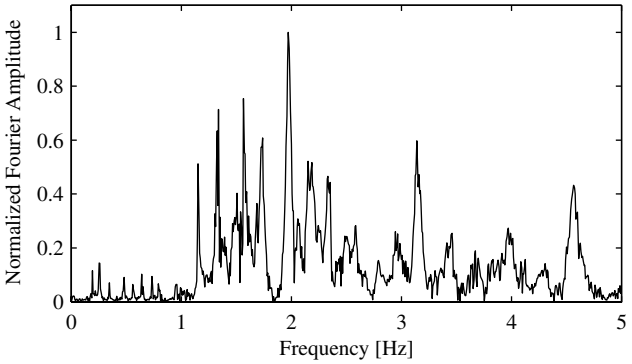

(a) Test No. 10

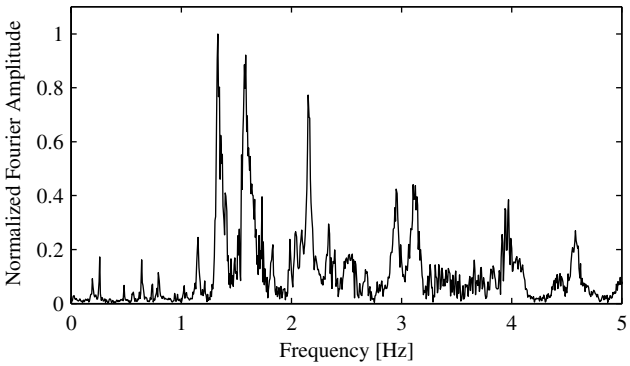

(b) Test No. 12

Fig. 9. Fourier amplitude spectra of vertical acceleration response at station 3SW measured in Tests No. 10 and 12

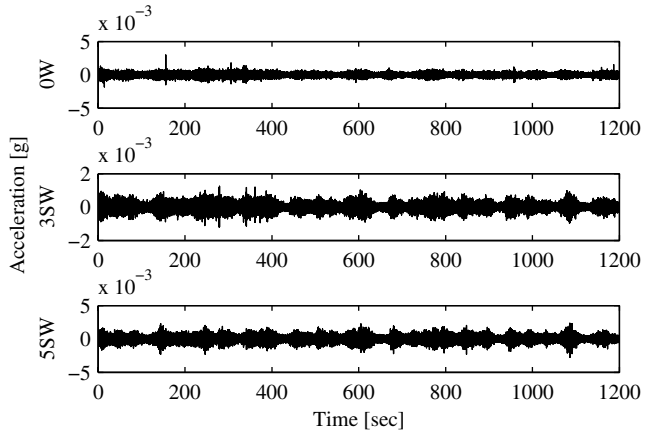

Fig. 10. Vertical bridge deck acceleration response measured in Test No. 18

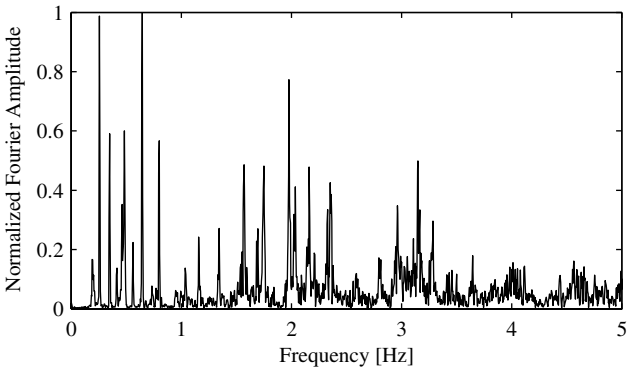

Fig. 11. Fourier amplitude spectrum of vertical acceleration response at station 3SW measured in Test No. 18

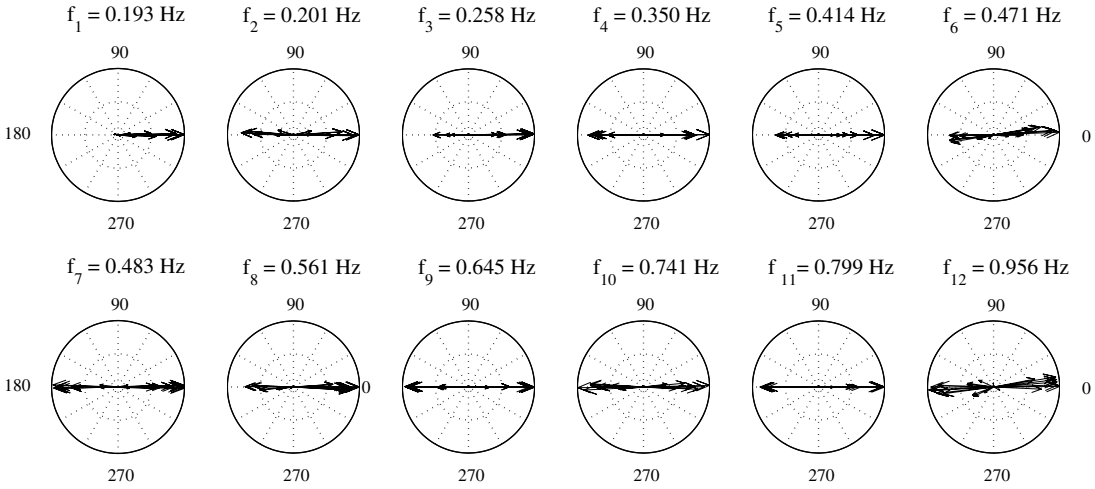

Fig. 12. Polar plot representation of vibration mode shapes identified using SSI-DATA

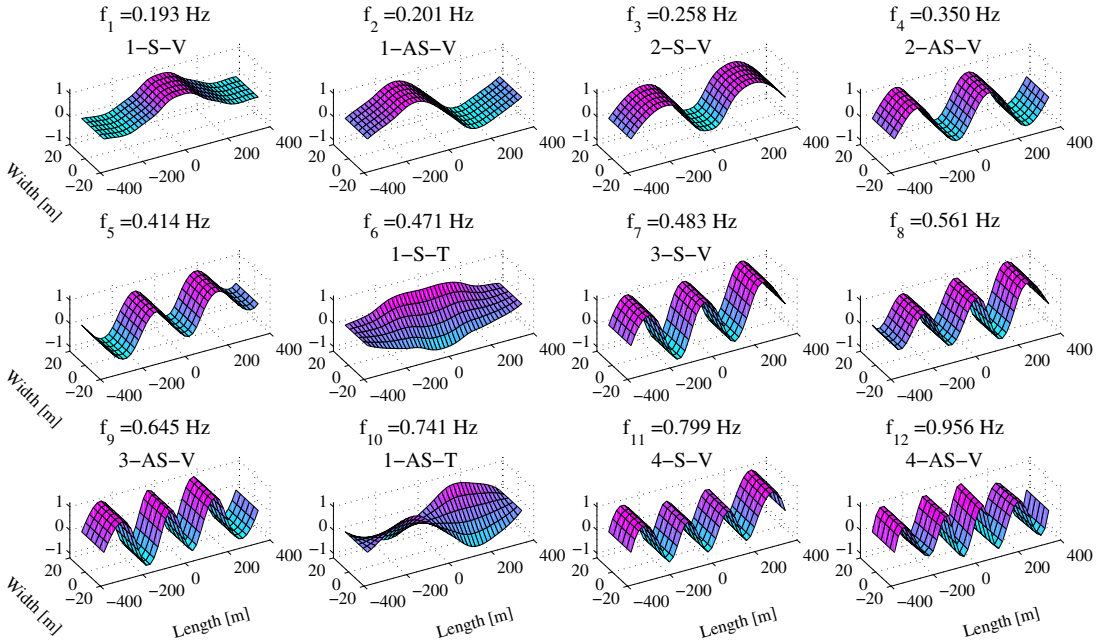

Fig. 13. 3D representation of normalized vibration mode shapes identified using SSI-DATA